Multiobjective optimization based on polynomial chaos expansions in the design of inductive power transfer systems

Yao Pei, Lionel Pichon, Mohamed Bensetti, Yann Le Bihan

Multiobjective Optimization based on Polynomial Chaos Expansions in the Design of Inductive Power Transfer Systems

Yao PEI, Lionel PICHON, Mohamed BENSETTI and Yann LE BIHAN

Université Paris-Saclay, CentraleSupélec, CNRS, Laboratoire de Génie Electrique et Electronique de Paris, 91192, Gif-sur-Yvette, France;

Sorbonne Université, CNRS, Laboratoire de Génie Electrique et Electronique de Paris, 75252, Paris, France.

E-mail: yao.pei@centralesupelec.fr

Abstract. In this paper, a new methodology combining the Polynomial Chaos Expansions (PCE) and a controlled, elitist genetic algorithm (GA) is proposed to design inductive power transfer systems. The relationship between the quantities of interest (mutual inductance and ferrite volume) and structural parameters (ferrite dimensions) is expressed by a PCE metamodel. Then, two objective functions corresponding to mutual inductance and ferrite are defined, and the other is the ferrite volume equation. These are combined with GA to obtain optimal parameters with a trade-off between these outputs. In addition, a sensitivity analysis directly available with this PCE metamodel shows how the structural parameters influence the outputs, which is helpful in choosing the final optimized values. This new method is easy to be implemented in Matlab, and can provide the Pareto front at a low computational cost, compared to the multiobjective optimization with 3D Finite Element Methods (FEM).

Keywords: Inductive power transfer, multiobjective Optimization, polynomial chaos expansions.

1. INTRODUCTION

Recently, due to global warming and air pollution, electric vehicles (EVs) have been widely used. However, electro-mobility faces some challenges, such as battery life and troublesome cables. So, inductive power transfer (IPT) systems have attracted significant attention to expand the battery life and simplify the charging process [1-2]. To meet the needs of the EV industry, significant effort has been invested into the design of highly-effective IPT couplers.

To this end, several magnetic pad designs have been proposed and studied by using an analytical design approach or numerical simulations in the literature so far. To compare different designs of magnetic pads, many researchers have considered the coupling coefficient k [3-4], kQ factor (Q is the coils' quality factor), the power density [5], or the leakage field as a criterion. In [6], only three variables are considered for k without getting the Pareto front. In [7], the core loss is chosen as the objective function on double-D pads without studying the misalignment effect. Reference [8] only optimized the number of turns in the transmitter and receiver pads. In [5], the circular pad is optimized between the efficiency η and the power density. Reference [9] proposes a cost-efficiency optimization algorithm to determine the design of the transmitter in a dynamic wireless power transfer system. However, it did not consider the design of the receiver pad. In [10], the normalized Gaussian network is used on the distribution of the ferrite volume, and Non-dominated Sorting Genetic Algorithm II (NSGA-II) is to find a Pareto front between the coupling coefficient and leakage magnetic flux density, but it optimizes the ferrite shape without keeping the transfer efficiency.

Moreover, in the case of an optimization procedure, the large number of simulations involved in a parametric sweep can be time-consuming. Some researchers run sweeps of only the most important parameters through principal component analysis. Reference [11] and [12] showed how changing each parameter can affect the output power, and this helps to find the critical parameters in order to reduce the number of simulations. However, when the model is in a 3D environment, even only those important parameters are considered for the optimization, the computation time is still a big problem.

In this paper, we present a new approach to perform the multiobjective optimization of an IPT system in order to find an optimal design for a 3D IPT system at a low computational cost. First, the IPT coupler is studied with a 3D FEM model for a wide range of design parameter values. Secondly, a relationship between the output (mutual inductance M) and structural design parameter values (ferrite dimensions) is expressed by a polynomial chaos expansion (PCE) metamodel [13-14]. A combination between such a metamodel and an optimization algorithm avoids including a 3D full-wave model into an iterative loop. So it leads to a significantly faster approach. This is the novelty of this paper. Then, to maximize the transfer efficiency in a general case and at a low cost, two objective functions are defined. The first objective is to maximize the mutual inductance M, the second objective is to minimize the ferrite volume M. The ferrite volume is a key feature in inductive systems for electric vehicles. It has a direct impact on the price and performance. Hereafter, a controlled, elitist genetic algorithm is proposed to find the Pareto front between the mutual inductance M and the ferrite volume V.

2. INDUCTIVE POWER TRANSFER SYSTEMS

The scheme of an inductive power transfer system for electric vehicles is provided in Figure 1.

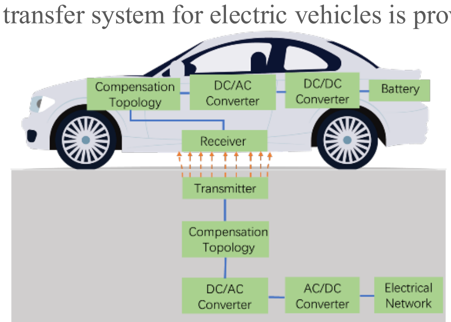

Figure 1: Scheme of an IPT system for electric vehicles

The power network feeds the transmitter through the converters and the compensation circuit. The receiver embedded at the bottom of the EV is used for picking up power from the magnetic field excited by the transmitter. In order to achieve a high transfer efficiency, a resonant compensation of the coupling coils is needed, such as series-series, parallel-parallel, series-parallel, parallel-series, and so on. Here, a resonant capacitor C_1 *or* C_2 is connected to the transmitter or the receiver in series, as shown in Figure 2 (R_1, R_2 represents the resistance of the wires, both in transmitter and receiver separately, M is the mutual inductance between the transmitter and the receiver, L_1, L_2 represents the self-inductances of the transmitter and receiver, R_L is the load) [15]. The working (resonant) frequency f_0 for this IPT system is 85 kHz

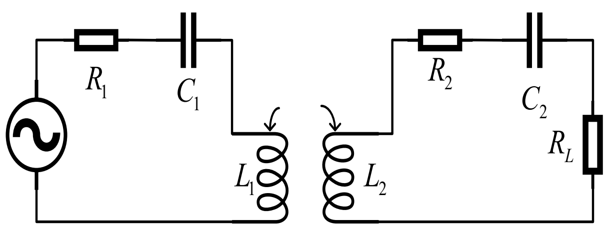

Figure 2. The equivalent electrical circuit in the series-series topology [1, 2, 13, 15]

Therefore, the equation to calculate the maximum transfer efficiency η_{max} can be simplified as below when $kQ \gg 1$, and the coils are identical for the transmitter and the receiver [17]:

$$\eta_{max} = \frac{(kQ)^2}{\left(1+\sqrt{1+(kQ)^2}\right)^2} \approx 1 - \frac{2}{kQ} = 1 - \frac{\sqrt{R_1 R_2}}{\pi f_0 M} = 1 - \frac{R_1}{\pi f_0 M} \qquad (1)$$

where the coupling coefficient is $k = \frac{M}{\sqrt{L_1 L_2}}$ and the system quality factor is $Q = 2\pi f_0 \sqrt{\frac{L_1 L_2}{R_1 R_2}}$.

Considering the transfer efficiency and tolerance to the misalignment, a lot of different coil geometries have been proposed, such as circular, square, bipolar, double-D, and so on [1-2,15,17]. Here, in Figure 3, the transmitter and receiver are square coils and made of Litz wires. The ferrite pad is used to decrease the magnetic flux leakage and improve the mutual inductance. The parameters of the coils and the ferrite pads are described in Table 1, and the permeability of the ferrite is 2500. However, the shielding problem is rarely considered in the early phase of a design process, which may result in the suboptimal operation of the entire system [18].

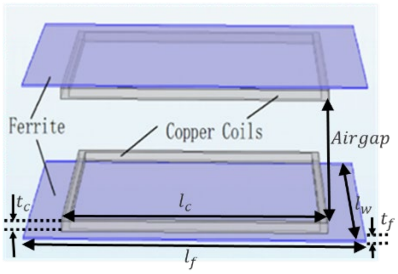

Figure 3: Base IPT system [4, 13]

Parameter	Value
Coil length l_c	468 mm
Coil thickness t_c	13mm
Ferrite length l_f	600 mm
Ferrite width l_w	500 mm
Ferrite thickness t_f	2 mm
Air gap	150 mm

Table 1: Structural parameters of the base IPT system

From Equation [1], the maximum transfer efficiency η_{max} is only related to the mutual inductance M between the transmitter and the receiver when the resonance frequency and the coils are fixed. So, the mutual inductance M is selected as one of the objective functions for efficiency optimization. When improving the mutual inductance M, the cost of ferrite also needs to be controlled. So the ferrite volume V becomes the other objective function.

3. Polynomial Chaos Expansions

Polynomial chaos expansions (PCE) are a powerful metamodeling technique that aims at providing a functional approximation of a computation model through its spectral representation on a suitably built basis of polynomial functions [14]. In this paper, the input parameters $\boldsymbol{X}$ are geometric values of the ferrite and the distance between the coil and ferrite, which are independent of each other. The PCE metamodel of the mutual inductance M is built on the outputs from 3D FEM modeling computations for the given range of parameters $\boldsymbol{X}$.

$$\widehat{\boldsymbol{M}}(\boldsymbol{X}) = \sum_{\alpha \in \mathcal{A}} c_\alpha \Phi_\alpha(\boldsymbol{X}) \tag{2}$$

where $\Phi_\alpha(\boldsymbol{X})$ are multivariate polynomials, the c_α are the corresponding coefficients, the multi-index α identifies the components of the multivariate polynomials Φ_α, the set $\mathcal{A}$ (which selects multi-indices of multivariate polynomials) is constructed on the hyperbolic truncation scheme that can be used to significantly reduce the cardinality of the polynomial basis [14].

Then, the leave-one-out (LOO) error is used to evaluate the accuracy of the PCE metamodel for the mutual inductance M. The equation below consists of building N separate metamodels $\widehat{\boldsymbol{M}}^{PCE\setminus i}$, each one created on a reduced model evaluation $\boldsymbol{X}\setminus x^{(i)} = \{x^{(j)}, j = 1, \cdots, N, j \neq i\}$ and comparing its prediction on the excluded point $x^{(i)}$ with the real value $M(x^{(i)})$ from 3D FEM simulations. The LOO error can be written as [14]:

$$\epsilon_{LOO} = \frac{\sum_{i=1}^{N}\left(M(x^{(i)}) - \widehat{\boldsymbol{M}}^{PCE\setminus i}(x^{(i)})\right)^2}{\sum_{i=1}^{N}\left(M(x^{(i)}) - \frac{1}{N}\sum_{i=1}^{N} M(x^{(i)})\right)^2} \tag{3}$$

After, a PCE metamodel allows deriving post-processing of the model response at a negligible computational cost. The first two statistical moments of $\widehat{\boldsymbol{M}}(\boldsymbol{X})$ are the mean value and variance given as follows [14]:

$$\mathbb{E}\left[\widehat{\boldsymbol{M}}(\boldsymbol{X})\right] = c_0 \quad (4)$$
$$\mathbb{V}\left[\widehat{\boldsymbol{M}}(\boldsymbol{X})\right] = \sum_{\lambda \in \mathcal{A}, \lambda \neq 0} c_\lambda^2 \quad (5)$$

Moreover, the first-order PCE-based Sobol index S_i of the model response $\widehat{\boldsymbol{M}}(\boldsymbol{X})$ for the input random variable X_i can be estimated [19-20]:

$$S_i = \frac{Var_{X_i}[E_{X_{\sim i}}[\widehat{\boldsymbol{M}}(\boldsymbol{X})|X_i]]}{\mathbb{V}[\widehat{\boldsymbol{M}}(\boldsymbol{X})]} = \frac{\sum_{\lambda \epsilon \mathcal{A}_i} c_\lambda^2}{\mathbb{V}[\widehat{\boldsymbol{M}}(\boldsymbol{X})]} \quad (6)$$

with $\mathcal{A}_{\mathrm{i}} = \{\lambda \epsilon \mathcal{A}: \lambda_i > 0, \lambda_j = 0\ \forall j \neq i\}$ and $\boldsymbol{X}_{\sim i}$ notation indicates the set of all variables except X_i.The total PCE-based Sobol indices $S_{T,i}$ can also be formulated as follow [19-20], which is the sum of all the Sobol' indices involving the i^{th} variable:

$$S_{T,i} = \frac{E_{X_{\sim i}}[Var_{X_i}[(\widehat{\boldsymbol{M}}(\boldsymbol{X})|\boldsymbol{X}_{\sim i})]]}{\mathbb{V}[\widehat{\boldsymbol{M}}(\boldsymbol{X})]} = \frac{\sum_{\lambda \epsilon \mathcal{A}_{T,i}} c_\lambda^2}{\mathbb{V}[\widehat{\boldsymbol{M}}(\boldsymbol{X})]} \quad (7)$$

where $\mathcal{A}_{\mathrm{T,i}} = \{\lambda \epsilon \mathcal{A}: \lambda_i \neq 0\}$.

The Sobol indices here are used to perform an efficient sensitivity analysis for Section 5. When the total Sobol indices and the first-order sobol index are equal, it means that the considered variables have no interactions with each other. In addition, the first-order PCE-based Sobol index of the i^{th} variable is closer to 1 means that the i^{th} variable has more impact on the PCE metamodel $\widehat{\boldsymbol{M}}(\boldsymbol{X})$. In this paper, the first-order Sobol indices can help to choose the final optimal parameters for the PCE metamodel $\widehat{\boldsymbol{M}}(\boldsymbol{X})$ during the multiobjective algorithm. The process to build an accurate PCE metamodel of the mutual inductance $\widehat{\boldsymbol{M}}(\boldsymbol{X})$ is shown in Figure 4.

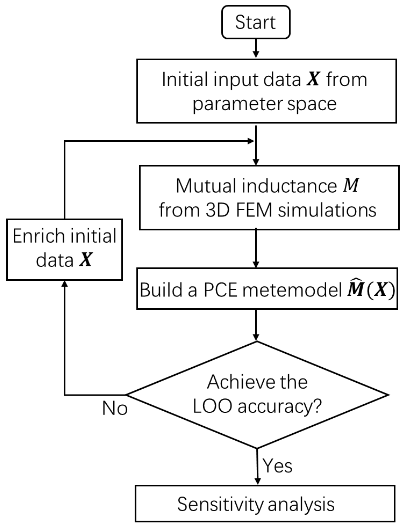

Figure 4: Process of PCE metamodel $\widehat{\boldsymbol{M}}(\boldsymbol{X})$

4. MULTIOBJECTIVE ALGORITHM

In this work, a controlled, elitist genetic algorithm (a variant of Non-dominated Sorting Genetic Algorithm II) is adopted in order to solve the multiobjective optimization problem [21]. The objective functions are defined as:

$$\widehat{\boldsymbol{M}}_{PCE}(\boldsymbol{X}) = max(M) : \text{To maximize the mutual inductance} \quad (8)$$

$$V_{ferrite}(\boldsymbol{X}) = min(V) : \text{To minimize the volume of the ferrite} \quad (9)$$

The progress of the optimization algorithm is shown in Figure 5. This algorithm evaluates the objective function and constraints for the population and uses those values to create scores for the population. It runs within MATLAB 2019 while the objective value of the mutual inductance is obtained by using the PCE metamodel, and the value of the ferrite volume is based on its volume equation. Here, the Pareto fraction is set as 0.3, which limits the number of individuals on the Pareto front. The number of individuals in the population is 100, and the generations are 200.

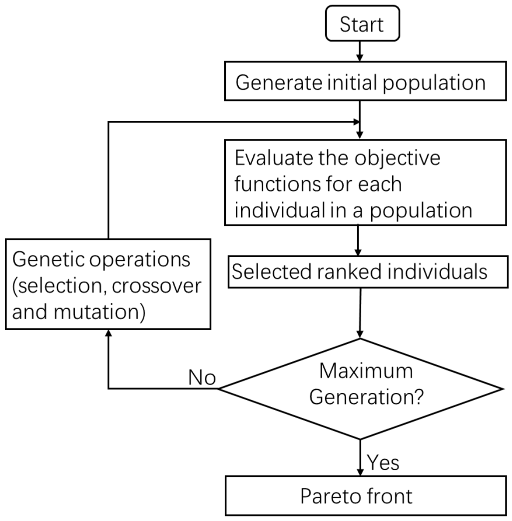

Figure 5: Process of multiobjective genetic algorithm

5. OPTIMIZATION PROBLEMS AND RESULTS

The proposed optimization based on PCE metamodel was achieved for inductive couplers with two identical square power pads. The FEM simulations run in a work station (XEON E5-1629). According to the number of individuals and the generations defined for the optimization algorithm in Section 4, it needs to run 20000 times in a 3D environment (COMSOL V5.6). At the same time, for the model in Section 5.1, the mesh consists of 199475 elements, and it costs 59 s for calculating one set of parameters; for the model in Section 5.2, the mesh consists of 289870 elements, and it costs 88 s for calculating one set of parameters. So if the optimization progress runs in a 3D environment, it may cost 328 hours (for the Section 5.1 model) or 489 hours (for the Section 5.2 model), which is quite time-consuming. However, for building an accurate PCE metamodel of the mutual inductance M, it requires at least 100 times of calculations from the 3D environment, which costs at least 2.4 hours. But the evaluation of M based on the PCE metamodel requires 1~2 seconds in Intel(R) Core(TM) i5-8365U (CPU @ 1.60GHz 1.90 GHz). Then, the optimization process based on PCE metamodel costs around 15 minutes. So compared to a conventional optimization based on the 3D model, it is easier to get optimized results with this approach, and it saves a lot of computation time. The results of the optimization process and the performance of the misalignment, and the leakage magnetic flux density on the design are discussed below.

5.1 GEEPS PRACTICAL IPT SYSTEM OPTIMIZATION

Here, the practical IPT configuration developed by GeePs and Vedecom institute is shown in Figure 6, and previous structure parameters are in Table 2 [22-23]. It is considered to be characterized by these five independent parameters listed in Table 3. A PCE metamodel is established to simulate the varying trend of the mutual inductance M.

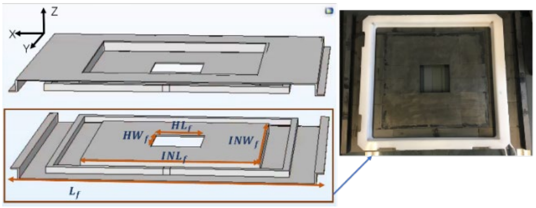

Figure 6: Practical IPT configuration [22-23]

Structural Parameter	Value
Ferrite length L_f	600 mm
Inner ferrite length INL_f	350 mm
Inner ferrite width INW_f	350 mm
Hole length HL_f	100 mm
Hole width HW_f	100 mm

Table 2: Previous parameters of the studied IPT configuration

Table 3: Structural parameters of the practical IPT configuration

Parameter Number	Structural Parameter	Min (mm)	Max (mm)	Probability density distribution
1	Ferrite length L_f	500	600	Uniform
2	Inner ferrite length INL_f	300	400	
3	Inner ferrite width INW_f	300	400	
4	Hole length HL_f	50	150	
5	Hole width HW_f	50	150	

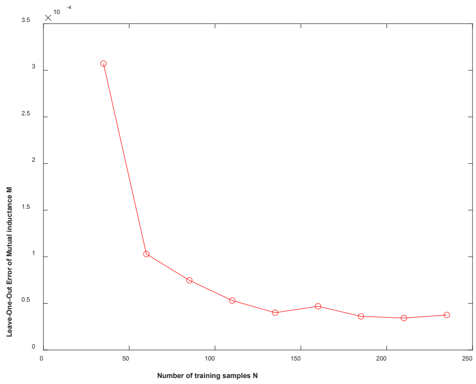

Figure 7: Leave-one-out error with number of training samples N

The training dataset generated by using the FEM solvers is selected by Latin Hypercube sampling [24]. In Figure 7, it is clear that LOO error decreases with the number of training samples increasing. To make a balance between LOO error and the computation time, 135 samples are chosen in this work to build an accurate PCE metamodel of the mutual inductance.

From Figure 8, it can be seen that the number of samples to build the PCE metamodel does not change the impact of the structural parameters on the mutual inductance M. Then, the total Sobol indices and first-order Sobol index have the same results, and it means that the structure parameters are independent of each other, which conforms to the condition in Section 3. Furthermore, the first-order Sobol index expresses that the ferrite length is the most important parameter to the mutual inductance M among these input parameters, which will be helpful for the multiobjective optimization in the next step.

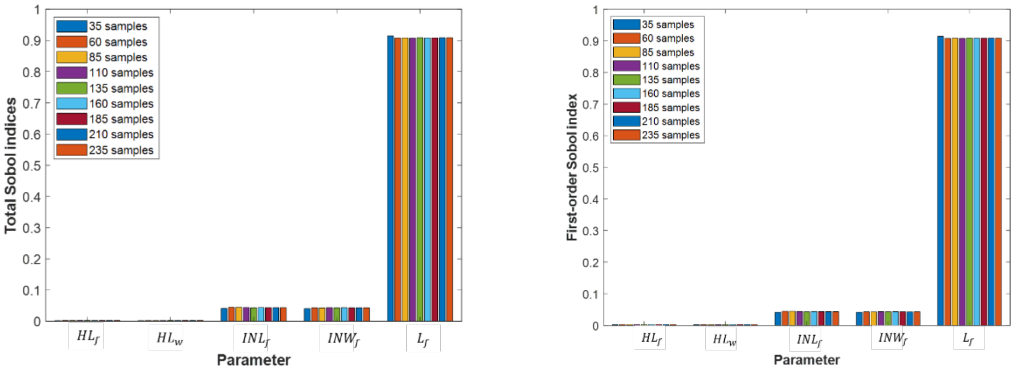

Figure 8: Sobol indices of mutual inductance M on practical IPT system

Then, the Pareto front of the multiobjective optimization based on the PCE metamodel $\widehat{\boldsymbol{M}}$ and the equation of ferrite volume V is shown in Figure 9. It can be seen that the mutual inductance M increases with the ferrite volume V increasing. The red point represents the previous values on the basis of Table 2. Although the points on the Pareto front satisfy the compromise between the objective functions above, the criterion is to select the solutions that M is not lower and V is not bigger than these of the redpoint. So the blue point is picked, which gives a higher M and smaller V.

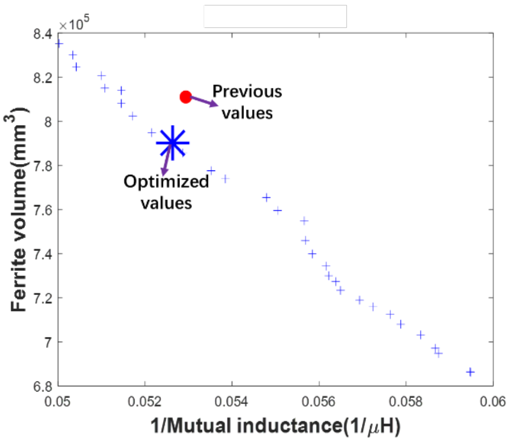

Figure 9: Pareto front between $1/M$ and B_{max} for the practical IPT system

The optimized parameters of this practical IPT configuration are shown in Table 4. It saves 44156 mm^3 of ferrite, which means it decreases nearly 3% of the previous ferrite volume from Table 2.

To evaluate the performance of the IPT system, a comparison between the mutual inductance M and the magnetic flux density B_{max} near the system obtained with the optimized values and the previous values is performed in case of misalignment during the charging process.

Table 4. Optimized values of the practical IPT configuration

Structural Parameter	Optimized Value
Ferrite length L_f	573 mm
Inner ferrite length INL_f	387 mm
Inner ferrite width INW_f	378 mm
Hole length HL_f	114 mm
Hole width HW_f	126 mm

Figure 10 shows that the mutual inductance M nearly keeps the same as that with the previous values, no matter which misalignment along the X or Y axis happens.

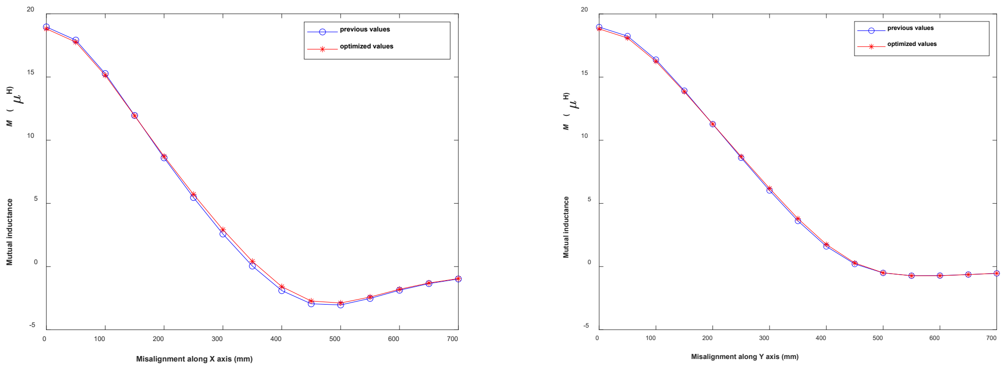

Figure 10: Variation of the mutual inductance M with the variation of the misalignment

The leakage magnetic flux density amplitude B_{max} (unit: μT) which is determined along a vertical line at 800 mm from the center of the coupling coils in Figure 12, and the optimized values are both smaller than 27μT (unperturbed RMS values) and meet the ICNIRP regulations [26]. However, B_{max} with the optimized values is smaller than that with the previous values, even if the misalignments happen.

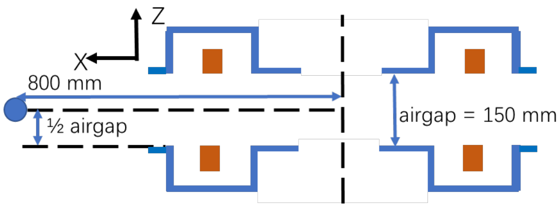

Figure 11: Measurement point for the magnetic flux density B_{max}

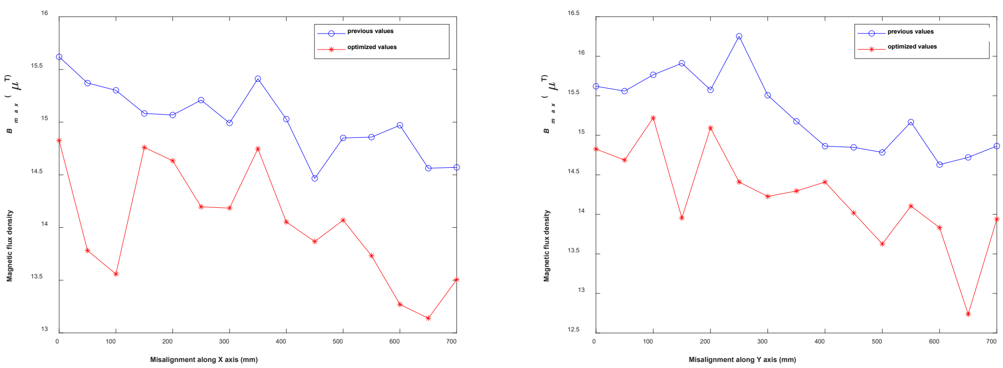

Figure 12: Variation of the magnetic flux density B_{max} with the variation of the misalignment

5.2 General Ferrite Design for IPT system Optimization

In general, the ferrite pad in many IPT systems consists of a rectangular or square plate, just like shown in Figure 13. However, finding how to choose the design dimensions of the ferrite plate (length, width, and thickness) is a difficult task. There is no general criteria or rule to help in this choice for a given coil size. So it is meaningful to find the relationship between the coil size and the ferrite size. The ranges of structural parameters are considered in Table 5 when the side of the square coil size is 468 mm studied in the GeePs before [4, 13, 23].

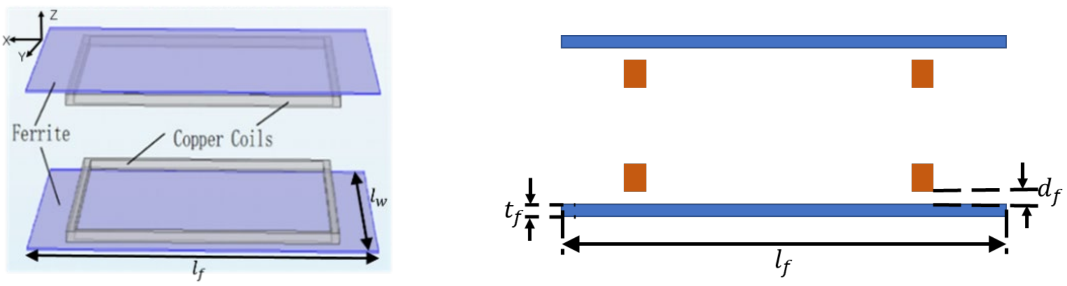

(a) General view *(b) Cross-sectional view*

Figure 13: IPT pad structure illustrating the design variables

Table 5: Structural parameters of the ferrite plate

Parameter Number	**Structural Parameter**	**Min (mm)**	**Max (mm)**	**Probability density distribution**
1	Ferrite length l_f	468	936	Uniform
2	Ferrite width l_w	468	936	
3	Ferrite thickness t_f	2	10	
4	Distance between coil and ferrite d_f	1	10	

The PCE metamodel for the mutual inductance $\widehat{\boldsymbol{M}}$ on this ferrite pad is based on 116 training samples, and the LOO error is 3.12e-6. Then, considering the sensitivity analysis for the mutual inductance and the ferrite volume in Figure 14, the total Sobol indices and the first-order Sobol index are identical, which expresses that these structural parameters are independent of each other and conforms to the conditions in Section 3. Moreover, for the mutual inductance M, the length and width of ferrite are quite important, but for the ferrite volume V, the ferrite thickness is the most important for the given ranges of values. This result will help to find an optimal value during the optimization procedure.

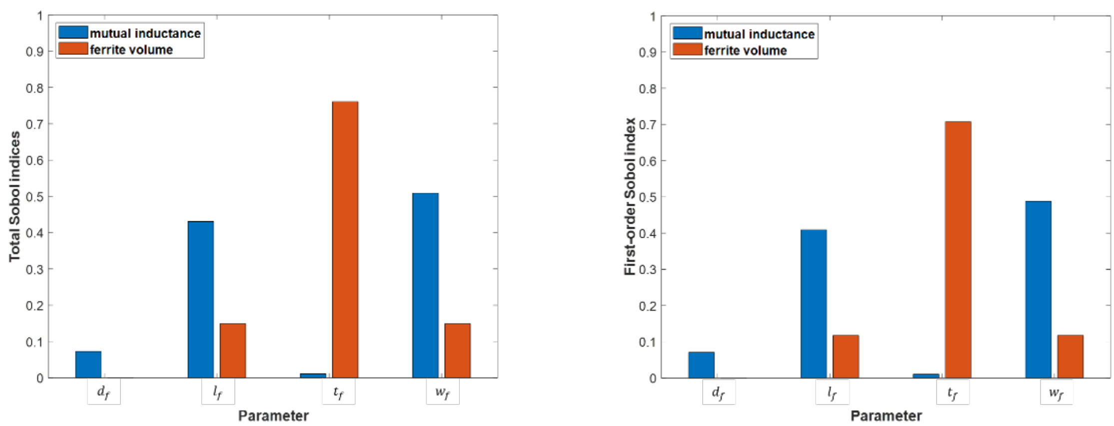

Figure 14: Sobol indices of mutual inductance M and ferrite volume V

After using the multiobjective optimization algorithm from Section 3, the Pareto front between the reciprocal of the mutual inductance and the ferrite volume is displayed in Figure 15.

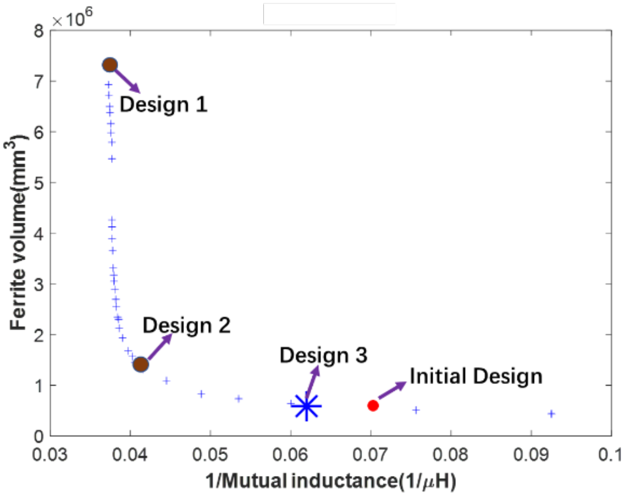

Figure 15: Pareto front between 1/M and V for a general rectangular IPT system

Table 6: Structural parameters of the ferrite plate

Design Number	Ferrite length l_f (mm)	Ferrite width w_f (mm)	Ferrite thickness t_f (mm)	Distance between coil and ferrite d_f (mm)	Mutual inductance M (μH)	One ferrite volume V (mm^3)
1	928	870	9	1.2	27.2	72.7e5
2	781	784	2	1.5	24.1	12.2e5
3	541	536	2	1.2	15.9	5.8e5
Initial	600	500	2	8.0	14.2	6.0e5

In Table 6, design 1 significantly improves the mutual inductance but leads to the most ferrite volume. Compared to the initial design, all the designs improves the mutual inductance, but only design 3 decreases nearly 3% of ferrite. In the studies above, it appears that design 2 may be the best choice because it locates at the knee point, which is normally considered first at the Pareto front. At the same time, the mutual inductance can also be further improved by changing the structure of ferrite, as described in Section 5.1.

However, considering a practical system for an electric vehicle, a low ferrite volume and a high mutual inductance are preferred, especially for the receiver which is installed in the electric vehicle. Therefore, in order to make a trade-off between the mutual inductance M and ferrite volume V, design 2 can be used in the transmitter, and design 3 can be used to the receiver, as shown in Figure 16.

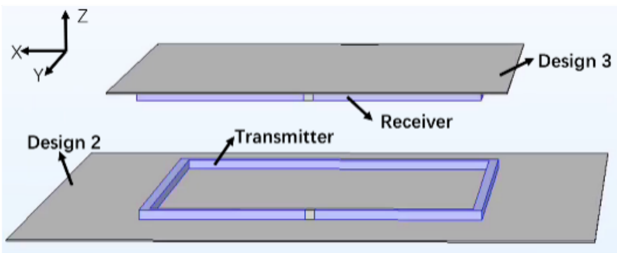

Figure 16: New ferrite arrangement for a general rectangular IPT system

The new ferrite arrangement improves the mutual inductance M and the tolerance to the misalignment, as shown in Figure 17. The leakage magnetic flux density B_{max} at the same point as in Figure 10 is 15.3 μT, which also meets the ICNIRP regulations.

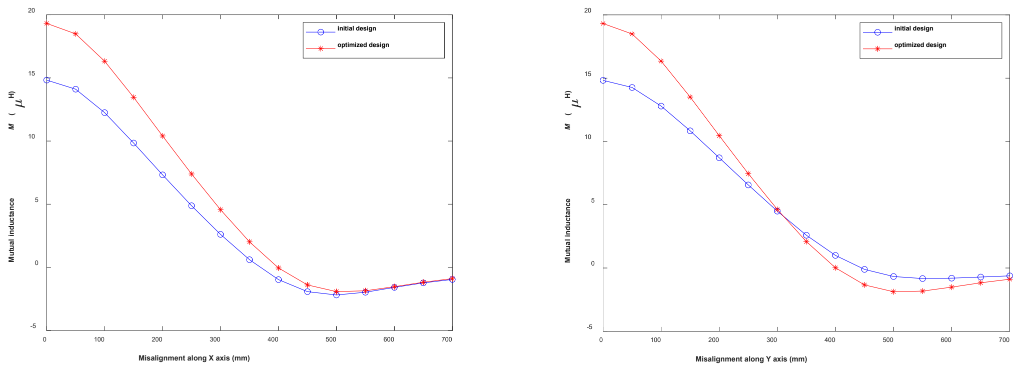

Figure 17: Variation of the mutual inductance M with the variation of the misalignment with new ferrite arrangement

6. CONCLUSION

In this paper, a multiobjective optimization based on polynomial chaos expansions has been applied to the design of inductive power transfer systems considering both the mutual inductance and ferrite volume. Using PCE metamodels to represent the mutual inductance and a controlled, elitist genetic algorithm for the optimization, the Pareto front has been successfully obtained. In the case of a practical IPT system, with the optimized values set inside, the mutual inductance is shown to be nearly the same as the previous situation (shown in Table 2), and it saves nearly 3% of ferrite volume. It demonstrates that the configuration of this practical IPT system is well designed. In the case of a general rectangular IPT system, it is shown that the size of the ferrite pad can be decided with the coil side through this approach. Finally, such a multiobjective optimization based on polynomial chaos expansions could be helpful to perform the optimization when considering the system in a realistic 3D environment involving many parameters. The variability in the shapes of ferrite pads will be considered in future work.

REFERENCES

[1] Ahmad, A., Alam, M. S., and Chabaan, R. (2018) "A Comprehensive Review of Wireless Charging Technologies for Electric Vehicles", *IEEE Transactions on Transportation Electrification*, 4(1), pp. 38–63. doi: 10.1109/TTE.2017.2771619.

[2] Panchal, C., Stegen, S. and Lu, J. (2018) "Review of static and dynamic wireless electric vehicle charging system", *Engineering Science and Technology, an International Journal*, 21(5), pp. 922–937. doi: 10.1016/j.jestch.2018.06.015.

[3] Yang, Y., Cui, J. and Cui, X. (2020) "Design and Analysis of Magnetic Coils for Optimizing the Coupling Coefficient in an Electric Vehicle Wireless Power Transfer System", Energies, 13(16), pp. 1–15. Available at: https://ideas.repec.org/a/gam/jeners/v13y2020i16p4143-d397479.html (Accessed: 25 May 2021).

[4] Kadem, K. et al., 2021. "Optimal Coupler Topology for Dynamic Wireless Power Transfer for Electric Vehicle". *Energies*, 14(13), p.3983. Available at: http://dx.doi.org/10.3390/en14133983.

[5] Bosshard, R. et al. (2015) "Modeling and η-α-Pareto Optimization of Inductive Power Transfer Coils for Electric Vehicles", IEEE Journal of Emerging and Selected Topics in Power Electronics, 3(1), pp. 50–64. doi: 10.1109/JESTPE.2014.2311302.

[6] Yao, Y. *et al.* (2021) "Design and Optimization of an Electric Vehicle Wireless Charging System Using Interleaved Boost Converter and Flat Solenoid Coupler", *IEEE Transactions on Power Electronics*, 36(4), pp. 3894–3908. doi: 10.1109/TPEL.2020.3019441.

[7] Mohammad, M., Choi, S. and Elbuluk, M. E. (2019) "Loss Minimization Design of Ferrite Core in a DD-Coil-Based High-Power Wireless Charging System for Electrical Vehicle Application", *IEEE Transactions on Transportation Electrification*, 5(4), pp. 957–967. doi: 10.1109/TTE.2019.2940878.

[8] Li, Y. *et al.* (2019) "A New Coil Structure and Its Optimization Design With Constant Output Voltage and Constant Output Current for Electric Vehicle Dynamic Wireless Charging", *IEEE Transactions on Industrial Informatics*, 15(9), pp. 5244–5256. doi: 10.1109/TII.2019.2896358.

[9] Gong, Y., Otomo, Y. and Igarashi, H. (2020) "Multiobjective topology optimization of magnetic couplers for wireless power transfer", *International Journal of Applied Electromagnetics and Mechanics*, 64(1–4), pp. 325–333. doi: 10.3233/JAE-209337.

[10] Tavakoli, R. et al. (2021) "Cost-Efficiency Optimization of Ground Assemblies for Dynamic Wireless Charging of Electric Vehicles", IEEE Transactions on Transportation Electrification, pp. 1–1. doi: 10.1109/TTE.2021.3105573.

[11] Budhia, M., Covic, G. A. and Boys, J. T. (2011) "Design and Optimization of Circular Magnetic Structures for Lumped Inductive Power Transfer Systems", IEEE Transactions on Power Electronics, 26(11), pp. 3096–3108. doi: 10.1109/TPEL.2011.2143730.

[12] Budhia, M. *et al.* (2013) "Development of a Single-Sided Flux Magnetic Coupler for Electric Vehicle IPT Charging Systems", *IEEE Transactions on Industrial Electronics*, 60(1), pp. 318–328. doi: 10.1109/TIE.2011.2179274.

[13] Pei, Y. *et al.* (2020) "Uncertainty quantification in the design of wireless power transfer systems", *Open Physics*, 18(1), pp. 391–396. doi: 10.1515/phys-2020-0174.

[14] *Polynomial chaos expansions (PCE) | User Manuals* (no date) *uqlab*. Available at: https://www.uqlab.com/pce-user-manual (Accessed: 9 September 2021).

[15] Cirimele, V. (2017) "Design and integration of a dynamic IPT system for automotive applications". PhD thesis. Université Paris Saclay; Politecnico di Torino. Available at: https://tel.archives-ouvertes.fr/tel-01578716 (Accessed: 10 November 2020).

[16] J2954: Wireless Power Transfer for Light-Duty Plug-in/Electric Vehicles and Alignment Methodology - SAE International (no date). Available at: https://www.sae.org/standards/content/j2954_202010/ (Accessed: 26 March 2021).

[17] Pei, Y. et al., (2021). "Comparison of Coupling Coils for Static Inductive Power-Transfer Systems Taking into Account Sources of Uncertainty". *Sustainability*, 13(11), p.6324. Available at: http://dx.doi.org/10.3390/su13116324.

[18] Yilmaz, T. *et al.* (2017) "Multiobjective Optimization of Circular Magnetic Couplers for Wireless Power Transfer Applications", *IEEE Transactions on Magnetics*, 53(8), pp. 1–12. doi: 10.1109/TMAG.2017.2692218.

[19] *Sensitivity analysis | User Manuals* (no date) *uqlab*. Available at: https://www.uqlab.com/sensitivity-user-manual (Accessed: 9 September 2021).

[20] Saltelli, A. et al. (2010) 'Variance based sensitivity analysis of model output. Design and estimator for the total sensitivity index', Computer Physics Communications, 181(2), pp. 259–270. doi:10.1016/j.cpc.2009.09.018.

[21] Deb, K. *et al.* (2000) "A Fast Elitist Non-dominated Sorting Genetic Algorithm for Multiobjective Optimization: NSGA-II", in Schoenauer, M. et al. (eds) *Parallel Problem Solving from Nature PPSN VI*. Berlin, Heidelberg: Springer (Lecture Notes in Computer Science), pp. 849–858. doi: 10.1007/3-540-45356-3_83.

[22] Bensetti, M. Et al., (2020). "Inductive Coupler and Magnetic Induction Charging System for Electric and hybrid Vehicles". FR3094832A1, WO2020208313A1.

[23] Kadem, K. (2020) "Modeling and Optimization of a magnetic coupler for dynamic induction charging of electric vehicles". PhD thesis. Université Paris-Saclay. Available at: http://www.theses.fr/s174545 (Accessed: 10 November 2020).

[24] McKay, M. D., Beckman, R. J. and Conover, W. J. (1979) "A Comparison of Three Methods for Selecting Values of Input Variables in the Analysis of Output from a Computer Code", *Technometrics*, 21(2), pp. 239–245. doi: 10.2307/1268522.

[25] Luo, Z. et al. (2021) "Multiobjective Optimization of Inductive Power Transfer Double-D Pads for Electric Vehicles", IEEE Transactions on Power Electronics, 36(5), pp. 5135–5146. doi: 10.1109/TPEL.2020.3029789.

[26] International Commission on Non-Ionizing Radiation Protection (2010) , "Guidelines for limiting exposure to time-varying electric and magnetic fields (1 Hz to 100 kHz)," *Health Phys*., vol. 99, no. 6, pp. 818–836, 2010.